

Synthesis of Colloidal SU-8 Polymer Rods Using Sonication

Carla Fernández-Rico,* Taiki Yanagishima, Arran Curran, Dirk G. A. L. Aarts, and Roel P. A. Dullens*

The bulk synthesis of fluorescent colloidal SU-8 polymer rods with tunable dimensions is described. The colloidal SU-8 rods are prepared by shearing an emulsion of SU-8 polymer droplets and then exposing the resulting non-Brownian rods to ultrasonic waves, which breaks them into colloidal rods with typical lengths of 3.5–10 μm and diameters of 0.4–1 μm . The rods are stable in both aqueous and apolar solvents, and by varying the composition of apolar solvent mixtures both the difference in refractive index and mass density between particles and solvent can be independently controlled. Consequently, these colloidal SU-8 rods can be used in both 3D confocal microscopy and optical trapping experiments while carefully tuning the effect of gravity. This is demonstrated by using confocal microscopy to image the liquid crystalline phases and the isotropic–nematic interface formed by the colloidal SU-8 rods and by optically trapping single rods in water. Finally, the simultaneous confocal imaging and optical manipulation of multiple SU-8 rods in the isotropic phase is shown.

Colloidal dispersions of rod-like particles are widely accepted as convenient model systems to study the phase behavior of liquid-crystal (LC) forming systems.^[1] This is due to the fact that colloidal rods exhibit analogous phase behavior to that of elongated molecules, while they can be directly observed by optical microscopy.^[1,2] Almost 70 years ago, Onsager already predicted that a system of hard rods undergoes an entropy-driven isotropic–nematic phase transition upon increasing the rod concentration.^[3] Since then, a great deal of theoretical and experimental work has been done on identifying and studying the key parameters influencing the LC phase behavior of rods, see, e.g., refs. [2,4–8]. Computer simulations have shown that systems of hard (spher)ocylinders can also exhibit smectic, columnar, and crystalline phases depending on their volume fraction, aspect ratio, and size polydispersity.^[4–7] Experimentally, much insight has been gained by studying colloidal rod-like model systems such as tobacco mosaic virus (TMV)

and fd-virus particles,^[8–10] poly(methyl methacrylate) (PMMA) ellipsoids,^[11,12] boehmite rods,^[13] and silica rods.^[14,15]

Detailed insight into the 3D structure and dynamics of dense colloidal phases at the particle level can be obtained using 3D confocal microscopy.^[16–18] This technique has also been applied to study dense suspensions of rods including fd-virus particles,^[19,20] PMMA ellipsoids,^[21,22] and silica rods.^[14,23] Using fd-virus particles, for example, the director fields of colloidal liquid crystals in wedge-shaped confinement was measured by adding fluorescent fd-virus particles in a host suspension of nonfluorescent fd-virus particles.^[19] Confocal microscopy was also used to study the structure of sediments of PMMA ellipsoids,^[21,22] the phase behavior of silica rods external fields,^[14,23,24] and the

structure of sedimentation–diffusion equilibria in mixtures of silica spheres and rods^[25] at the single particle level.

Confocal microscopy, however, does put severe constraints on the colloidal model system to be used. First, the refractive index of the particles needs to be matched to that of the dispersing solvent ($\Delta n \approx 0$) in order to minimize scattering effects when imaging deep into the bulk of concentrated samples. Second, it is beneficial to be able to tune the effect of gravity by adjusting the mass density difference between the particles and the solvent, $\Delta\rho$. In this way, for instance, fluctuating interfaces,^[26] sedimentation–diffusion equilibria ($\Delta\rho > 0$),^[27] or the 3D structure of crystalline phases ($\Delta\rho \approx 0$)^[28,29] can be monitored over time using the same colloidal particles. For rods specifically, the small dimensions of the fd-viruses and the high mass density of silica rods make tuning the effect of gravity in these systems cumbersome. While this is possible for PMMA ellipsoids, they are typically produced in low yields and deviate from the ideal rod-like shape, as a result of which smectic, columnar, or crystalline phases have not been observed in concentrated suspensions of these ellipsoids.^[21]

Here, we describe the bulk synthesis of fluorescent colloidal SU-8 polymer rods with tunable length and diameter that are stable in both aqueous and apolar solvent mixtures. By varying the composition of the solvent mixture, both the difference in refractive index and mass density between the particles and the solvent can be independently controlled. This enables the use of colloidal SU-8 rods in both 3D confocal microscopy ($\Delta n \approx 0$) and optical trapping ($\Delta n \neq 0$) experiments, and even in experiments combining both techniques. Crucially, the effect of gravity can be carefully tuned in all of these experiments via $\Delta\rho$. We demonstrate this by imaging the liquid crystalline phases

C. Fernández-Rico, Dr. T. Yanagishima, Dr. A. Curran, Prof. D. G. A. L. Aarts, Prof. R. P. A. Dullens
Department of Chemistry
Physical and Theoretical Chemistry Laboratory
University of Oxford
South Parks Road, Oxford OX1 3QZ, UK
E-mail: carla.fernandezrico@chem.ox.ac.uk; roel.dullens@chem.ox.ac.uk

 The ORCID identification number(s) for the author(s) of this article can be found under <https://doi.org/10.1002/adma.201807514>.

© 2019 The Authors. Published by WILEY-VCH Verlag GmbH & Co. KGaA, Weinheim. This is an open access article under the terms of the Creative Commons Attribution-NonCommercial License, which permits use, distribution and reproduction in any medium, provided the original work is properly cited and is not used for commercial purposes.

DOI: 10.1002/adma.201807514

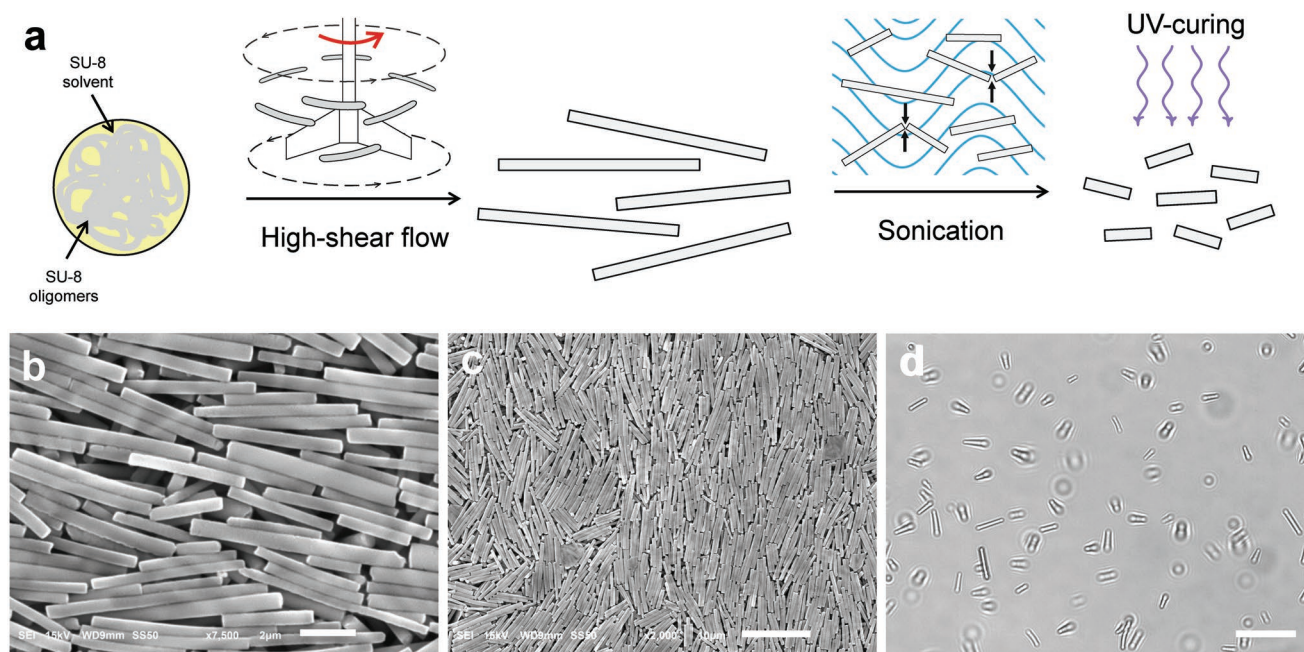


Figure 1. a) Schematic representation of the synthesis of the colloidal SU-8 polymer rods. Under high-shear flow, a macroscopic droplet of SU-8 polymer solution in glycerol is emulsified into smaller droplets that are subsequently elongated into cylinders of tens of micrometers long. Subsequent exposure to sonication breaks the long SU-8 rods into shorter colloidal SU-8 rods. Finally, exposing the rods to UV-light photo-crosslinks the SU-8 and yields chemically highly stable colloidal SU-8 rods. b–d) Scanning electron microscopy (SEM) images (b,c) and an optical microscopy image (d) of the colloidal SU-8 rods obtained at a shear stress of 518 Pa (see the Supporting Information) after a sonication period of 3 h. Scale bars are: b) 2 μm , c) 10 μm , and d) 20 μm .

and the isotropic–nematic interface formed by the colloidal SU-8 rods using confocal microscopy in various solvent mixtures. In addition, we show the optical trapping of single SU-8 rods in water and the simultaneous optical manipulation and confocal imaging of multiple rods in the isotropic phase.

To synthesize the fluorescent colloidal SU-8 polymer rods, we adapt the procedure for the fabrication of non-Brownian SU-8 rods described in refs. [30,31]. In that work, ten to a hundred micrometers long SU-8 rods were obtained by vigorously shearing an emulsion of SU-8 polymer droplets in a viscous medium. Here, we use sonication to break the non-Brownian SU-8 rods into smaller colloidal SU-8 rods, as shown schematically in Figure 1a. This simple yet crucial step opens up the use of SU-8 rods within the colloidal domain. To enable the imaging of the colloidal SU-8 polymer rods with 3D confocal microscopy, we incorporate a fluorescent dye (e.g., rhodamine) in the initial SU-8 photoresin (see the Supporting Information), which results in uniformly labeled and highly fluorescent colloidal SU-8 rods. Finally, UV-light exposure is used to crosslink the colloidal SU-8 rods, which yields chemically highly stable particles that can be dispersed in both aqueous and nonaqueous solvents.

Figure 1b,c shows typical scanning electron microscopy images of the colloidal SU-8 polymer rods obtained after sonication. First of all, the dimensions of the rods are clearly within the colloidal domain with an average length of $L \approx 4.5 \mu\text{m}$, diameter of $D \approx 0.5 \mu\text{m}$, and hence an aspect ratio of $L/D \approx 9$. While the rods are rather polydisperse, cycles of sedimentation and centrifugation in water can be used to reduce their size polydispersity down to $\approx 20\%$ in length, 15% in diameter, and 20% in aspect ratio (see the Supporting Information). Shapewise, the

obtained rods have an almost ideal cylindrical shape with flat ends, which is due to the sonication-induced breakage of the brittle SU-8 rods that are obtained after the shearing process. Figure 1d shows an optical microscopy image of an aqueous dispersion of colloidal SU-8 rods, where the random positions and orientations are reminiscent of the translational and rotational Brownian motion exhibited by the colloidal rods as directly shown in Movie S1 in the Supporting Information.

The dependence of the average length, diameter, and aspect ratio of the SU-8 rods on the sonication time is shown in Figure 2. Importantly, there is a clear decrease in the average rod length, especially during the first hour of sonication, while the rod diameter remains roughly constant. However, the rod diameter can be independently tuned from 0.4 up to 1 μm during the first step of the synthesis where increasing the applied shear stress leads to thinner rods^[30,31] (see the Supporting Information). The aspect ratio of the colloidal SU-8 rods can thus be fully tuned by the duration of the sonication. Interestingly, the change in the distributions in Figure 2d–f shows that the length reduction during sonication is mainly driven by the breakage of the initially long rods into shorter rods due to the violent implosion of the cavitation bubbles created during sonication.^[32,33] Indeed, the peaks of the length and aspect ratio distributions shift toward smaller values and the tails of both distributions are greatly reduced. This is also reflected by the decrease of the standard deviation in the mean values, represented by the error bars in Figure 2g–i. We note that the sonication time required for the rods to reach their final average length depends on the sonication parameters: increasing the power or decreasing the sonication frequency leads to faster

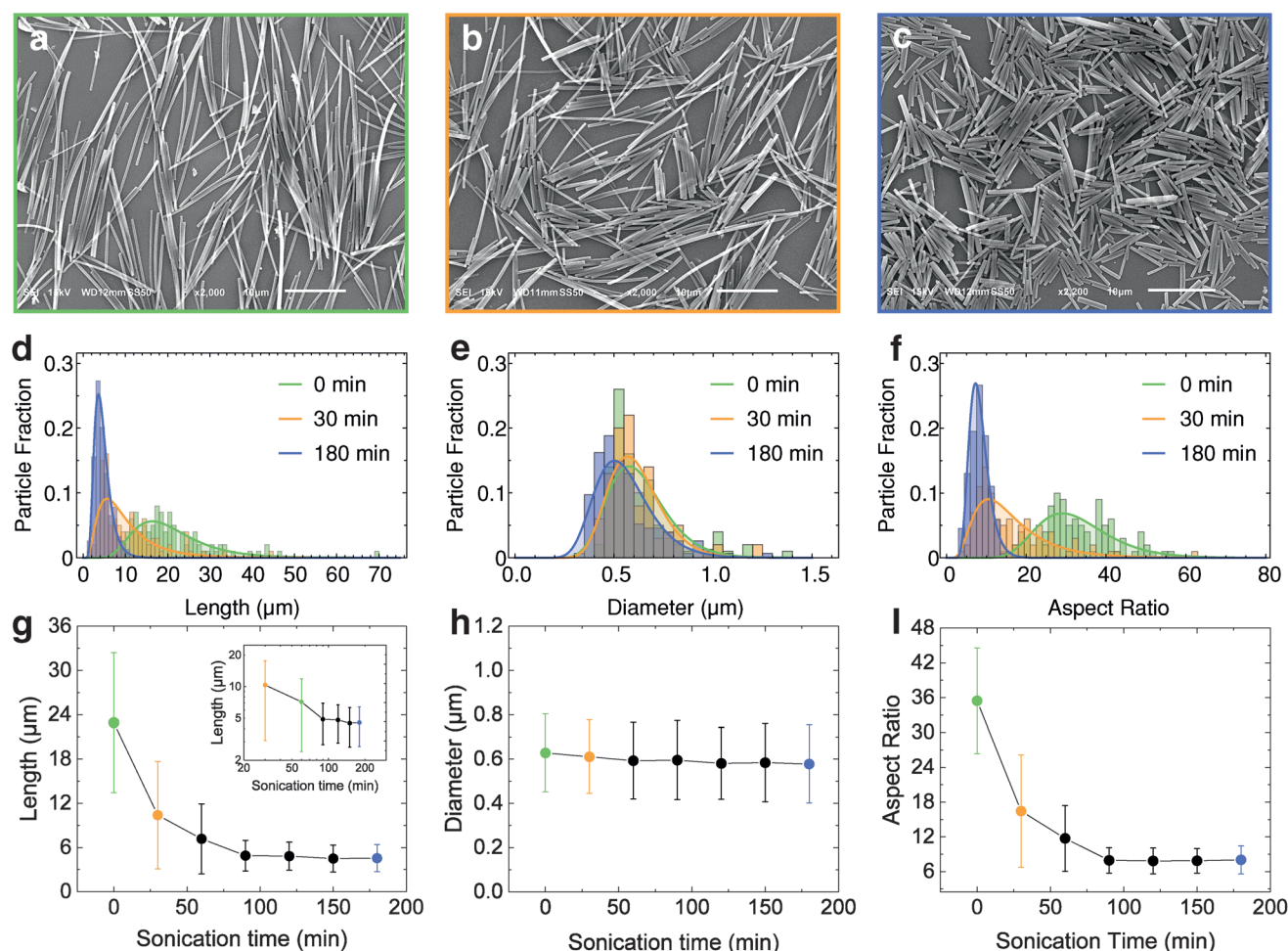


Figure 2. a–c) Representative SEM images of the SU-8 rods before (a) and after 30 min (b) and 180 min (c) of sonication. Scale bars are 20 μm . d–f) Length, diameter, and aspect ratio distributions of the SU-8 rods at 0, 30, and 180 min of sonication. g, h) Evolution of the average length, diameter, and aspect ratio of SU-8 rods as a function of the sonication time. Inset: log–log plot of length as a function of the sonication time. The error bars represent the standard deviation of the average value.

rod-breakage (see the Supporting Information).^[32,33] While the dimensions of the colloidal SU-8 rods synthesized in this paper are optimized for their study with 3D confocal microscopy, we anticipate that the minimum rod-dimensions could be further reduced by increasing the shear stress applied during the first step of the synthesis or decreasing the SU-8 polymer concentration of the initial SU-8 solution as discussed in ref. [31].

Stable aqueous dispersions of colloidal SU-8 rods in water are obtained by adding small amounts of ionic (SDS) or non-ionic (Pluronic F-108) surfactants (see the Supporting Information). The resulting colloidal stability is further confirmed by the observed self-assembly of the colloidal SU-8 rods in water into various liquid crystalline phases, as shown in **Figure 3**. In order to form these phases, we slightly tilt the sample, thereby inducing a packing fraction gradient. At low packing fractions, the rods exhibit no translational or orientational ordering, reminiscent of the isotropic phase, while at higher packing fractions, the rods orient in the same direction corresponding to nematic ordering (Figure 3b). At even higher packing fractions, the rods self-assemble into a smectic-like structure (Figure 3c). This may seem surprising as the typical rod-length polydispersity of the

SU-8 rods $\approx 30\%$ is above the terminal polydispersity of 18%, where the smectic phase is predicted to no longer be stable for a system of hard spherocylinders.^[6] However, a rod-length count performed in the smectic-like phase shows that the local length-polydispersity has significantly decreased to about 20% due to fractionation,^[34,35] which facilitates the formation of a smectic-like phase like the one shown in Figure 3c.

To observe the structure and dynamics of the colloidal SU-8 rods using 3D confocal microscopy, the refractive index of the particles and the solvent mixture should be closely matched ($\Delta n \approx 0$), while ideally the degree of mass density matching, $\Delta \rho$, is carefully controllable. With the literature values for the refractive index and mass density of bulk SU-8 photoresin being $n \approx 1.59$ and $\rho \approx 1.2 \text{ g mL}^{-1}$,^[36] this can be readily achieved by dispersing the rods into common organic solvent mixtures akin to those used for matching PMMA and 3-(trimethoxysilyl)propyl methacrylate (TPM) particles.^[29,37] To determine the refractive index and mass density of our colloidal SU-8 rods—that is, after shearing and UV curing (see Figure 1a)—we disperse the rods in carefully prepared mixtures of organic solvents with different compositions and

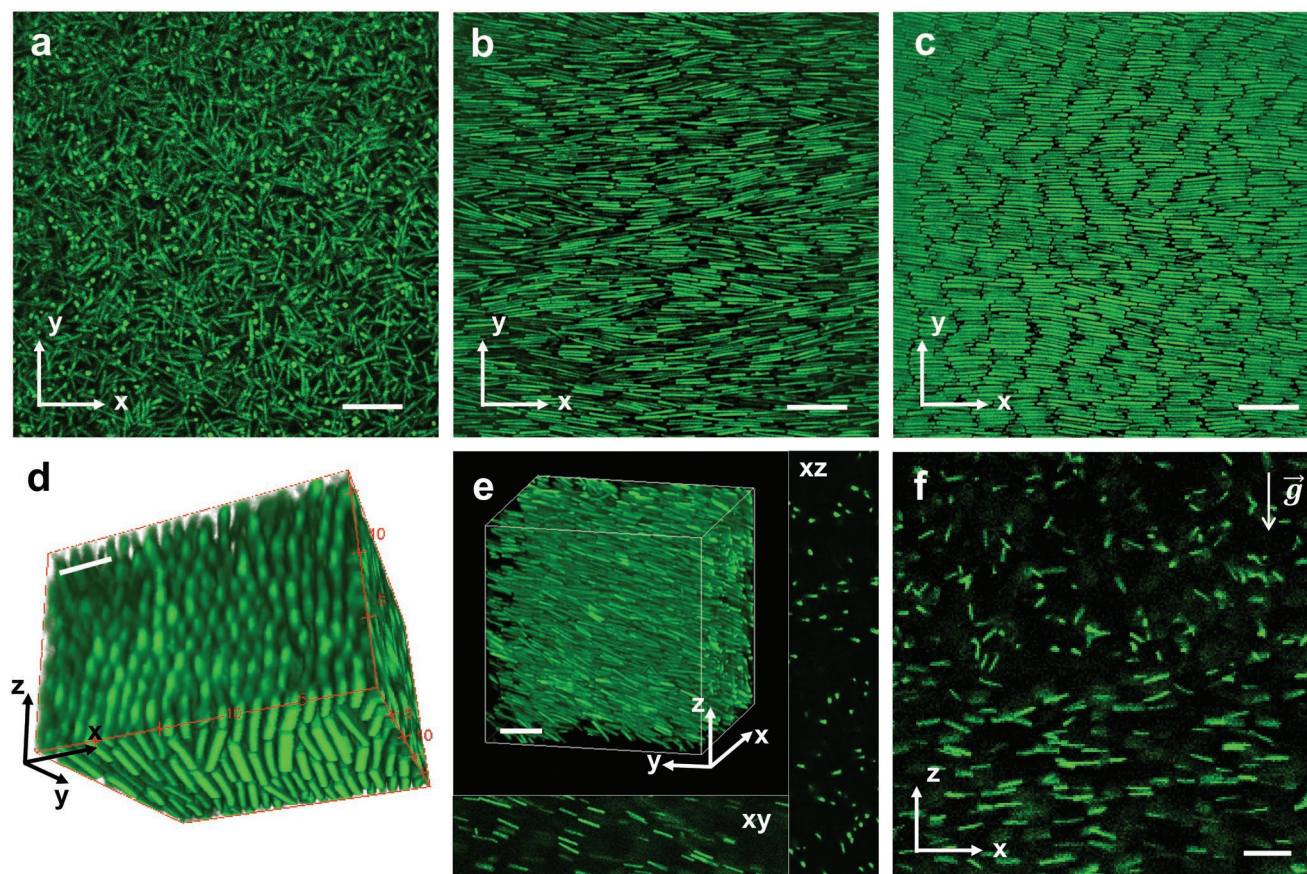


Figure 3. a–c) Confocal microscopy images of a tilted sample containing an aqueous dispersion of fluorescent SU-8 rods with $L = 5.3 \mu\text{m}$ ($\sigma_L = 29.1\%$), $D = 0.62 \mu\text{m}$ ($\sigma_D = 16.1\%$), $L/D = 8.8$ ($\sigma_{D/L} = 29.5\%$): a) isotropic, b) nematic, and c) smectic-like ordering upon increasing volume fraction. d) 3D confocal image ($20 \times 20 \times 17 \mu\text{m}^3$) of the nematic phase of fluorescent colloidal SU-8 rods in tetralin ($L_g \approx 2 \mu\text{m}$). e) 3D confocal image ($50 \mu\text{m}^3$) of the nematic phase of a 1:50 mixture of fluorescent and nonfluorescent colloidal SU-8 rods in a 1:11 mixture of TCE:CS₂ ($L_g \approx 200 \mu\text{m}$). The side and bottom panels show the xy and xz cross-sections, respectively. f) Confocal image of an isotropic–nematic interface of a 1:30 mixture of fluorescent and nonfluorescent colloidal SU-8 rods in a 1:4 DEC:CS₂ ($L_g \approx 6 \mu\text{m}$). Scale bars are $10 \mu\text{m}$.

hence different refractive indices and mass densities (see the Supporting Information).^[14,29,38,39] The dispersants OLOA-1200 or OLOA-11000 are used to stabilize the rods in these organic solvents.^[29,40] By identifying the maximum optical transparency and the transition point between sedimentation and creaming, the refractive index and mass density of the colloidal SU-8 rods are found to be $n = 1.614$ and $\rho \approx 1.28 \text{ g mL}^{-1}$. Conveniently, with these values, various mixtures of common organic solvents (see Table 1) can be used to independently, and hence simultaneously or not, match the refractive index

and the mass density of the colloidal SU-8 rods. This allows the effect of gravity, as quantified by the gravitational length of the rods, $L_g = k_B T / V_p \Delta \rho g$, to be systematically varied from ≈ 1 up to $\approx 200 \mu\text{m}$ in nearly refractive index matched dispersions. Here, $k_B T$ is the thermal energy, V_p is the volume of the rods, and g is the acceleration due to gravity.

The controllability of gravity in our colloidal SU-8 rod system is demonstrated in Figure 3d–f, where 3D confocal microscopy images of rods with different gravitational lengths are shown. Figure 3d shows a 3D image of the fluorescent rods in the

Table 1. Characteristics of typical solvent mixtures that can be used to tune the refractive index and mass density mismatch (Δn , $\Delta \rho$) between the particles and the solvent. The fraction of tetralin (TET), carbon disulfide (CS₂), trichloroethylene (TCE), and tetrachloroethylene (PERC) is given in v/v% ratios. The dimensions of the rod used to calculate L_g are $L = 5 \mu\text{m}$ and $D = 0.5 \mu\text{m}$.

Solvent	TET	CS ₂	TCE	PERC	Δn	$\Delta \rho [\text{g mL}^{-1}]$	$L_g [\mu\text{m}]$
1	1	0	0	0	0.073	0.314	1.4
2	1	5	0	0	0.001	0.067	6.3
3	1	0	1.6	0	0.112	0.012	34.3
4	1	0	0	0.9	0.089	0.005	82.8
5	0	11	1	0	−0.001	0.002	233.0

nematic phase in tetralin (solvent 1, Table 1), which demonstrates the imaging of all the particles at the single-particle level, where particle coordinates and orientations may potentially be extracted using existing images processing algorithms, as described in ref. [23]. In the Supporting Information, we provide Movie S2 showing the dynamics of the colloidal SU-8 rods in 3D in the nematic phase. Next, in Figure 3e, the composition of the solvent is such that both Δn and $\Delta \rho$ are very close to zero. Here, a 3D snapshot of the nematic phase formed in a 1:50 mixture of fluorescent and nonfluorescent colloidal SU-8 rods in solvent 5 is shown (note that $L_g \gg$ field of view). Since refractive index matching was almost perfect ($\Delta n \approx 0$), imaging of the rods was easily achieved 50 μm deep into the sample without significant loss of fluorescence intensity. Next, the mass density mismatch is increased to induce a sedimentation–diffusion equilibrium in which the L_g of the rods is tuned such that the isotropic–nematic interface can be directly observed as shown in Figure 3f. From a corresponding 3D confocal z-stack, we estimated the isotropic–nematic transition to occur at an approximate volume fraction of 0.25 (see the Supporting Information). While this value only represents a rough estimate, it

is comparable to earlier reports,^[15] and is also consistent with the value reported for hard spherocylinders at the appropriate aspect ratio.^[7] By systematically varying the effect of gravity on the rods, one could potentially study various interfacial properties of colloidal liquid crystals.^[41–43]

The versatility of our colloidal SU-8 rods warrants further applications in a wider range of experiments. The independent tunability of the refractive index and mass density mismatch facilitates, for example, the optical manipulation of the rods with, again, controllable effects of gravity. **Figure 4a** shows the dynamic manipulation of a colloidal SU-8 rod in water using two different optical traps acting on either end of the rod, which can, for example, be used to measure the friction coefficient of a rod as a function of its distance to the surface.^[44] In Figure 4b, we show preliminary results on the simultaneous confocal imaging and optical manipulation of a collection of SU-8 rods in the isotropic phase. This is achieved by choosing an organic solvent (solvent 1, Table 1) with a refractive index mismatch small enough to image tens of micrometers deep into the sample, but still large enough to use holographic optical tweezers to manipulate the particles.^[45]

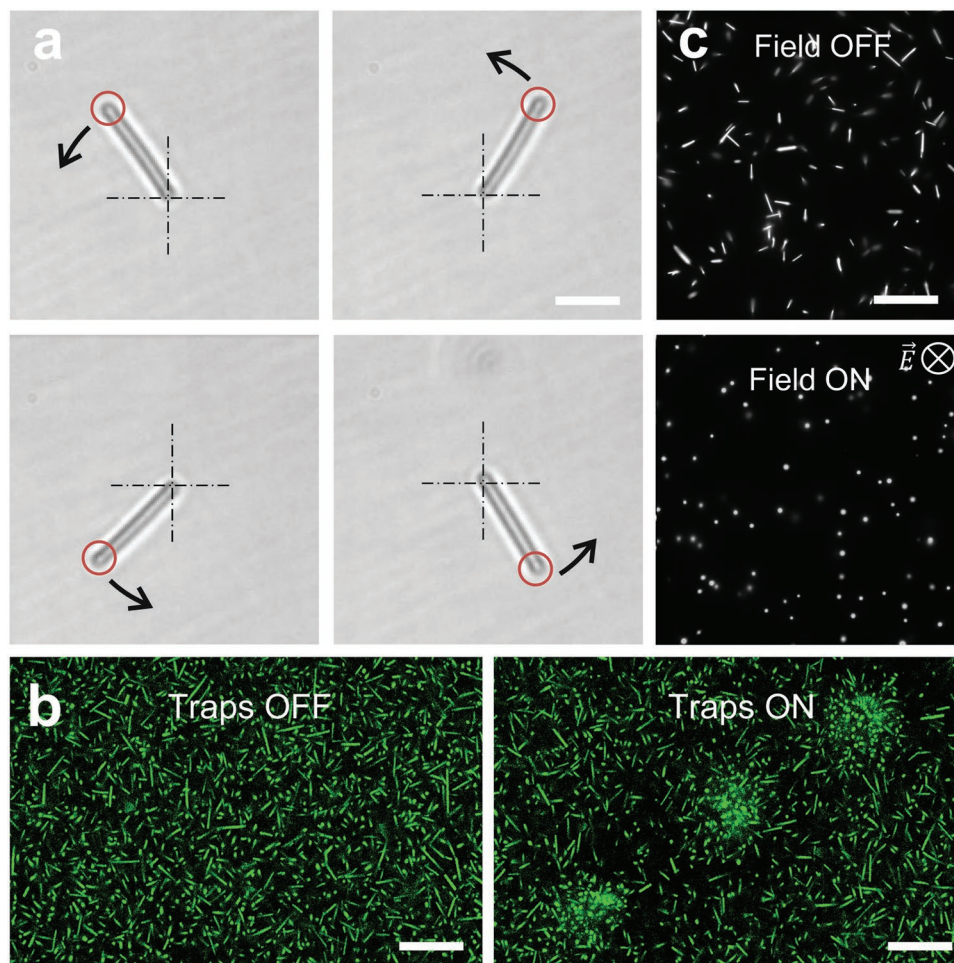


Figure 4. a) In-plane optical manipulation of a single SU-8 rod in water using two optical traps. b) Simultaneous optical manipulation and confocal imaging of a collection of colloidal SU-8 rods in tetralin using three independent optical traps. The optical axis of the traps is perpendicular to the image plane, which is 10 μm above the sample wall. c) Fluorescence microscopy images showing the effect of a 1 kHz AC electric field ($E \approx 0.01 \text{ V } \mu\text{m}^{-1}$) in a dilute dispersion of colloidal SU-8 rods. Scale bars are: a) 2 μm and b,c) 20 μm .

Interestingly, the three optical traps clearly induce local orientational (nematic) ordering, with the rods aligning along the optical axis,^[46] at higher packing fractions than that of the background isotropic phase. This effect may be exploited to study the nucleation of nematic droplets (tactoids) in the isotropic phase.^[47] In addition, we note that manipulating the isotropic–nematic interface using optical tweezers, in principle, also allows for the study of various interfacial phenomena, as was shown for the colloidal liquid–gas interface.^[48] Furthermore, we show that the colloidal SU-8 rods can also be aligned using external electric fields, see Figure 4c, as was also done for silica rods.^[14] Finally, we note that the composition, and hence the optical and chemical properties, of the colloidal SU-8 rods can be readily varied by incorporating other polymers and/or nanoparticles as reported in refs. [31,49]. In particular, the incorporation of silver or magnetic nanoparticles would make the rods conductive and/or magnetic which could be then used, for example, in sensing applications^[50,51] or studies of self-assembly in the presence of external magnetic fields.^[24]

In summary, we have shown the successful bulk synthesis of colloidal SU-8 polymer rods and its optimization for confocal microscopy and optical trapping experiments. The dimensions, composition, stability, and tunability of this system, as well as the ease of synthesis, combined with the wealth of knowhow available for tuning interparticle interactions in colloidal systems, promise a wide range of applications of colloidal SU-8 rods in condensed matter experiments.

Experimental Section

The synthesis of the colloidal SU-8 polymer rods was adapted from the method described by Alargova et al.^[30,31] In a typical synthesis, a 250 mL beaker with an inner diameter of 5 cm was filled with 110 mL of glycerol. A mixer (Heidolph RZR 2021) equipped with a high-shear impeller with a diameter of 3.5 cm was then introduced into the glycerol such that the impeller was located ≈ 2 cm above the bottom wall of the beaker. Once the homogenization process at 1500 rpm—corresponding to a shear stress of 518 Pa (see the Supporting Information)—was started, ≈ 0.1 g of SU-8 50 viscous photoresin (Microchem) was dropped from a spatula into the gap between the inner wall of the beaker and the impeller, resulting in a turbid dispersion. For the synthesis of fluorescent SU-8 rods, the dye was simply mixed with the SU-8 50 at a mass ratio of 10 mg dye g⁻¹ SU-8 50 (see the Supporting Information). The high-shear mixing of the glycerol and the SU-8 50 was continued for 10 min. The resulting non-Brownian SU-8 rod-like particles in glycerol were directly exposed to sonication (VWR ultrasonic cleaner, 45 kHz, 80 W) for 1–3 h to break them into smaller colloidal rods. These colloidal SU-8 rods were subsequently photo-crosslinked by exposing them to UV-light with a wavelength of 365 nm (Spectroline 14A/FB) for 30 min. To remove the glycerol, the colloidal SU-8 rods were washed by repeated centrifugation and redispersion cycles at $3000 \times g$ for 40 min using water containing 0.2 wt% SDS. Any large or irregularly shaped rods were easily removed by sedimentation in water under gravity for an hour. Very small rods were removed by centrifuging three times at $3000 \times g$ for 15 min. Long and thick rods were typically removed by spinning at $600 \times g$ for 15 min. Finally, the resulting colloidal SU-8 rods were kept in water containing 0.2 wt% SDS.

Further details on the fluorescent labeling, effect of shear stress and sonication parameters, sorting, refractive index, and mass density determination of the colloidal SU-8 rods, as well as on the confocal microscopy and optical manipulation experiments are given in the Supporting Information.

Supporting Information

Supporting Information is available from the Wiley Online Library or from the author.

Acknowledgements

The authors thank Louis Cortes, Adam Edward Stones, Lachlan Alexander, Paul van der Schoot, and Stefano Sacanna for useful discussion. The authors thank Eric Dufresne and Azelis for providing the OLOA-1200 and OLOA-11000, respectively. The ERC (ERC Consolidator Grant No. 724834 – OMCIDC) is acknowledged for financial support.

Conflict of Interest

The authors declare no conflict of interest.

Keywords

colloidal rods, confocal microscopy, optical tweezing, sonication, tunable gravity

Received: November 20, 2018

Revised: February 11, 2019

Published online: March 14, 2019

- [1] S. C. Glotzer, M. J. Solomon, *Nat. Mater.* **2007**, 6, 557.
- [2] H. N. W. Lekkerkerker, G. J. Vroege, *Philos. Trans. R. Soc., A* **2013**, 371, 20120263.
- [3] L. Onsager, *Ann. N. Y. Acad. Sci.* **1949**, 51, 627.
- [4] D. Frenkel, H. N. W. Lekkerkerker, A. Stroobants, *Nature* **1988**, 332, 822.
- [5] A. Stroobants, *Phys. Rev. Lett.* **1992**, 69, 2388.
- [6] M. A. Bates, D. Frenkel, *J. Chem. Phys.* **1998**, 109, 6193.
- [7] P. Bolhuis, D. Frenkel, *J. Chem. Phys.* **1997**, 106, 666.
- [8] Z. Dogic, S. Fraden, *Curr. Opin. Colloid Interface Sci.* **2006**, 11, 47.
- [9] M. P. Lettinga, E. Grelet, *Phys. Rev. Lett.* **2007**, 99, 2.
- [10] E. Grelet, *Phys. Rev. Lett.* **2008**, 100, 1.
- [11] K. M. Keville, E. I. Franses, J. M. Caruthers, *J. Colloid Interface Sci.* **1991**, 144, 103.
- [12] D. Mukhija, M. J. Solomon, *Soft Matter* **2011**, 7, 540.
- [13] P. A. Buining, C. Pathmamanoharan, J. B. H. Jansen, H. N. W. Lekkerkerker, *J. Am. Ceram. Soc.* **1991**, 74, 1303.
- [14] A. Kuijk, A. van Blaaderen, A. Imhof, *J. Am. Chem. Soc.* **2011**, 133, 2346.
- [15] A. Kuijk, D. V. Byelov, A. V. Petukhov, A. van Blaaderen, A. Imhof, *Faraday Discuss.* **2012**, 159, 181.
- [16] A. van Blaaderen, P. Wiltzius, *Science* **1995**, 270, 1177.
- [17] W. K. Kegel, A. van Blaaderen, *Science* **2000**, 287, 290.
- [18] V. Prasad, D. Semwogerere, E. R. Weeks, *J. Phys.: Condens. Matter* **2007**, 19, 113102.
- [19] O. J. Dammone, I. Zacharoudiou, R. P. A. Dullens, J. M. Yeomans, M. P. Lettinga, D. G. A. L. Aarts, *Phys. Rev. Lett.* **2012**, 109, 1.
- [20] A. H. Lewis, I. Garlea, J. Alvarado, O. J. Dammone, P. D. Howell, A. Majumdar, B. M. Mulder, M. P. Lettinga, G. H. Koenderink, D. G. A. L. Aarts, *Soft Matter* **2014**, 10, 7865.
- [21] A. Mohraz, M. J. Solomon, *Langmuir* **2005**, 21, 5298.
- [22] D. Mukhija, M. J. Solomon, *Soft Matter* **2011**, 7, 540.

- [23] T. H. Besseling, M. Hermes, A. Kuijk, B. de Nijs, T. S. Deng, M. Dijkstra, A. Imhof, A. van Blaaderen, *J. Phys.: Condens. Matter* **2014**, 27, 194109.
- [24] Y. Gao, F. Romano, R. P. A. Dullens, J. K. Doye, D. G. A. L. Aarts, *Phys. Rev. Mater.* **2018**, 2, 015601.
- [25] H. E. Bakker, S. Dussi, B. L. Droste, T. H. Besseling, C. L. Kennedy, E. I. Wiegant, B. Liu, A. Imhof, M. Dijkstra, A. van Blaaderen, *Soft Matter* **2016**, 12, 9238.
- [26] D. G. A. L. Aarts, M. Schmidt, H. N. W. Lekkerkerker, *Science* **2004**, 304, 847.
- [27] J. Hernández-Guzmán, E. R. Weeks, *Proc. Natl. Acad. Sci. USA* **2008**, 106, 15198.
- [28] U. Gasser, *Science* **2001**, 292, 258.
- [29] Y. Liu, K. V. Edmond, A. Curran, C. Bryant, B. Peng, D. G. Aarts, S. Sacanna, R. P. A. Dullens, *Adv. Mater.* **2016**, 28, 8001.
- [30] R. G. Alargova, K. H. Bhatt, V. N. Paunov, O. D. Velev, *Adv. Mater.* **2004**, 16, 1653.
- [31] R. G. Alargova, V. N. Paunov, O. D. Velev, *Langmuir* **2006**, 22, 765.
- [32] A. Lucas, C. Zakri, M. Maugey, M. Pasquali, P. van der Schoot, P. Poulin, *J. Phys. Chem. C* **2009**, 113, 20599.
- [33] Y. Y. Huang, T. P. Knowles, E. M. Terentjev, *Adv. Mater.* **2009**, 21, 3945.
- [34] G. J. Vroege, D. M. Thies-Weesie, A. V. Petukhov, B. J. Lemaire, P. Davidson, *Adv. Mater.* **2006**, 18, 2565.
- [35] E. van den Pol, D. M. Thies-Weesie, A. V. Petukhov, G. J. Vroege, K. Kvashnina, *J. Chem. Phys.* **2008**, 129, 164715.
- [36] S. K. Mitra, S. Chakraborty, *Microfluidics and Nanofluidics Handbook: Fabrication, Implementation, and Applications*, CRC Press, Boca Raton, FL, USA **2011**, p. 641.
- [37] P. N. Pusey, W. van Megen, *Nature* **1986**, 320, 340.
- [38] V. A. Tolpekin, M. H. Duits, D. van den Ende, J. Mellema, *Langmuir* **2004**, 20, 2614.
- [39] J. C. R. Reis, I. M. Lampreia, Á. F. Santos, M. L. C. Moita, G. Douhéret, *ChemPhysChem* **2010**, 11, 3722.
- [40] S. K. Sainis, V. Germain, C. O. Mejean, E. R. Dufresne, *Langmuir* **2008**, 24, 1160.
- [41] K. Shundyak, R. van Roij, *J. Phys.: Condens. Matter* **2001**, 13, 4789.
- [42] R. L. C. Vink, T. Schilling, *Phys. Rev. E* **2005**, 71, 1.
- [43] S. Wolfsheimer, C. Tanase, K. Shundyak, R. van Roij, T. Schilling, *Phys. Rev. E* **2006**, 73, 1.
- [44] R. Agarwal, K. Ladavac, Y. Roichman, C. M. Lieber, D. G. Grier, *Opt. Express* **2005**, 13, 1135.
- [45] A. Curran, S. Tuohy, D. G. A. L. Aarts, M. J. Booth, T. Wilson, R. P. A. Dullens, *Optica* **2014**, 1, 223.
- [46] J. L. Abbott, J. A. Spiers, Y. Gao, D. G. A. L. Aarts, R. P. A. Dullens, *J. Phys. D: Appl. Phys.* **2018**, 52, 024002.
- [47] A. Modlinska, A. M. Alsayed, T. Gibaud, *Sci. Rep.* **2015**, 5, 1.
- [48] A. A. Verhoeff, F. A. Lavergne, D. Bartolo, D. G. A. L. Aarts, R. P. A. Dullens, *Soft Matter* **2015**, 11, 3100.
- [49] S. K. Smoukov, T. Tian, N. Vitchuli, S. Gangwal, P. Geisen, M. Wright, E. Shim, M. Marquez, J. Fowler, O. D. Velev, *Adv. Mater.* **2015**, 27, 2642.
- [50] S. Jiguet, A. Bertsch, H. Hofmann, P. Renaud, *Adv. Funct. Mater.* **2005**, 15, 1511.
- [51] L. Chen, G. Chen, L. Lu, *Adv. Funct. Mater.* **2007**, 17, 898.